

# Multi-synchrosqueezing Transform

Gang Yu, Zhonghua Wang and Ping Zhao

**Abstract**— Time-frequency (TF) analysis (TFA) method is an important tool in industrial engineering fields. However, restricted to Heisenberg uncertainty principle or unexpected cross-terms, the classical TFA methods often generate blurry TF representation, which heavily hinder its engineering applications. How to generate the concentrated TF representation for a strongly time-varying signal is a challenging task. In this paper, we propose a new TFA method to study the non-stationary features of strongly time-varying signals. The proposed method is based on synchrosqueezing transform and employs an iterative reassignment procedure to concentrate the blurry TF energy in a step-wise manner, meanwhile retaining the signal reconstruction ability. Two implementations of the discrete algorithm are provided, which show that the proposed method has limited computational burden and has potential in real-time application. Moreover, we introduce an effective algorithm to detect the instantaneous frequency trajectory, which can be used to decompose mono-component modes. Numerical and real-world signals are employed to validate the effectiveness of the proposed method by comparing with some advanced methods. By comparisons, it is shown that, the proposed method has the better performances in addressing strongly time-varying signals and noisy signals.

**Index Terms**—Time-frequency analysis, multi-synchrosqueezing transform, signal reconstruction.

## I. INTRODUCTION

Time-frequency (TF) analysis (TFA) is an effective tool to analyze time-varying signals and has drawn considerable attention in the past few decades [1-2]. The classical linear methods, such as short time Fourier transform (STFT) and wavelet transform (WT), can expand a one-dimensional time-series signal into the two-dimensional (2D) TF plane. From the TF plane, we can observe time-varying features and perform signal decomposition. However, restricted by the Heisenberg uncertainty principle, TF representations generated via conventional methods are often blurry, and it is impossible to provide a precise TF description for a time-varying signal. The recent development of TFA methods involves designing high-resolution methods while retaining the ability to recover the original time-series signal [3]. Therefore, we can determine the time-varying features as detailed as possible and achieve the decomposition of the multi-component modes. The eventual development goal of the TFA techniques should be the ideal TFA (ITFA), which can be formulated as

Manuscript received March 24, 2018; revised June 19, 2018; accepted August 14, 2018. This work was supported in part by the National Natural Science Foundation of China under Grant 61374074 and Shandong Provincial Natural Science Foundation of China under Grant ZR2017JL028.

The authors are with the School of Electrical Engineering, University of Jinan, Jinan 250022, China (email: yugang2010@163.com).

Corresponding author contacts, phone: +86 150 6415 5055, e-mail: yugang2010@163.com.

$$ITFA(t, \omega) = \sum_{k=1}^K A_k(t) \delta(\omega - \varphi'_k(t)) e^{i\varphi_k(t)}. \quad (1)$$

where the  $\delta()$  denotes the Dirac delta function, which degenerates to Kronecker delta function in the discrete signal processing [4, 5]. The expression (1) is based on the multi-component non-stationary signal model

$$s(t) = \sum_{k=1}^K s_k(t) = \sum_{k=1}^K A_k(t) e^{i\varphi_k(t)} \quad (2)$$

where the  $A_k(t)$  is the instantaneous amplitude (IA),  $\varphi_k(t)$  denotes the instantaneous phase (IP), and its first-order derivative  $\varphi'_k(t)$  is the instantaneous frequency (IF). From (1), it is known that the ITFA representation possesses highly concentrated energy and appears only in the IF trajectories.

Unfortunately, the shortcomings of the conventional TFA methods heavily restrict their applications in real-world data processing. To improve the performance of conventional methods and to approach ITFA gradually, many advanced methods have been developed in the past few decades, e.g., the reassignment method (RM) [6], synchrosqueezing transform (SST) [7-9], demodulated SST (DSST) [10-13] and high-order SST [14-19].

The RM technique is designed to improve the readability of the original TF representation [6]. The main procedure of RM is to first calculate the newly reassigned positions for each TF point based on TF phase information. Then, the 2D reassignment operations (respectively, frequency reassignment and time reassignment) are employed to integrate the TF spectrogram in the TF direction. The RM technique inspires that the post-processing on the conventional TFA methods is an effective way to obtain a sharper TF result. However, the RM framework is based on a spectrogram, which means that the RM result loses its ability to reconstruct signal.

Just improving readability is not enough for real-world applications. Another recent technique, the SST, has brought new hope to achieve ITFA-like tools [7]. The SST method not only enhances the TF resolution, but also allows for reconstructing the signal. It has been proved that the SST result is equivalent to the ITFA representation when addressing a purely harmonic signal. However, many studies show that, when dealing with time-varying signals, e.g., chirp signals or nonlinear frequency-modulated (FM) signals, the SST cannot generate a concentrated TF result [8, 9]. This is because the frequency reassignment operator in the SST cannot provide an unbiased estimation for the true time-varying IF. How to obtain the more precise frequency reassignment operator is the most essential question to solve the problem in the SST method.

Linear TFA methods are to calculate the inner product between the signal and the basis function, which can locate the local time-varying features. Taking STFT for example, the

STFT framework is established on the assumption of the considered signal should be piece-wisely stationary in a short time. However, the analyzed time-varying signal cannot be guaranteed to always be stationary in a short time, e.g., a strong FM signal. According to the inner product theory, a more well-matched basis function with the time-varying signal can be more suitable for characterizing the TF features with concentrated energy [20]. Therefore, many non-linear TFA methods are proposed to address the strongly time-varying signals by demodulating the FM component [10-13]. Furthermore, it is found that the demodulated TF result can lead to a more precise frequency reassignment operator. Such methods, combining SST and the demodulated technique, show its effectiveness in generating highly energy-concentrated TF results [12, 13]. To demodulate a signal, we need to know the time-varying FM law of the signal in advance. However, due to the complexity and diversity of practical cases, determining the precise demodulated parameter is very difficult, especially for addressing signals with multiple FM components [11, 21].

In practice, the non-parametric and non-demodulated SST is more suitable for addressing real-world data. The authors proposed the second-order SST that can effectively provide high-resolution TF representation while retaining the reversible ability [14, 15]. Recently, the same group further proposed a higher-order SST that is designed to obtain more concentrated TF results [16]. However, the increasing SST order comes with a higher computational cost. For instance, the original SST needs to execute only one STFT operation, while the fourth-order SST requires executing eleven STFT operations.

In this paper, we present an iterative procedure that can effectively improve the energy concentration of the SST method in addressing strongly time-varying signals, meanwhile still allowing for perfect signal reconstruction. In theory, the proposed method belongs to the post-processing tool of the STFT. To derive this method, the STFT operation needs to be executed only once, such that it has a low computational cost. It does not require extra parameters or a priori information to demodulate the FM modes, which is more suitable for real-world applications. This paper is structured as follows. The theory of the proposed method are detailed in Section II. The numerical and experimental validations are provided in Section III and Section IV. The Discussion and conclusion are drawn in Section V and Section VI, respectively.

## II. MULTI-SYNCHROQUEEZING TRANSFORM

### A. Synchrosqueezing transform

In this section, we begin our study based on an STFT framework. The STFT of a function  $s \in L^2(\mathbb{R})$  with respect to the real and even window  $g \in L^2(\mathbb{R})$  is defined by

$$G(t, \omega) = \int_{-\infty}^{+\infty} g(u-t)s(u)e^{-i\omega(u-t)} du \quad (3)$$

where the window  $g(u)$  compactly supports in  $[-\Delta_t, \Delta_t]$ . We first consider the mono-component signal model

$$s(t) = A(t)e^{i\varphi(t)}. \quad (4)$$

In theory, the STFT is to calculate the Fourier transform of

$g(u-t)s(u)$  in the short time  $u \in [t-\Delta_t, t+\Delta_t]$ . Herein, it is necessary to assume that  $\exists \varepsilon$  sufficient small,  $|A'(t)| \leq \varepsilon$  and  $|\varphi''(t)| \leq \varepsilon$  for  $\forall t$ . With this assumption, the signal (4) can be approximately regarded as the purely harmonic signal in a short time. According to the Taylor expansion, we can expand the  $A(u)$  and  $\varphi(u)$  at the time point  $t$ . The related expressions are written as  $A(u) = A(t)$  and  $\varphi(u) = \varphi(t) + \varphi'(t)(u-t)$ , where the terms on the order  $O(A'(t))$  and  $O(\varphi''(t))$  are neglected. Therefore, the signal (4) can be expressed as

$$s(u) = A(t)e^{i(\varphi(t) + \varphi'(t)(u-t))}. \quad (5)$$

The signal (5) is substituted into STFT, and then we have

$$\begin{aligned} G(t, \omega) &= \int_{-\infty}^{+\infty} g(u-t)A(t)e^{i(\varphi(t) + \varphi'(t)(u-t))} e^{-i\omega(u-t)} du \\ &= A(t)e^{i\varphi(t)} \int_{-\infty}^{+\infty} g(u-t)e^{i(\varphi'(t)(u-t) - i\omega(u-t))} d(u-t) \\ &= A(t)e^{i\varphi(t)} \hat{g}(\omega - \varphi'(t)) \end{aligned} \quad (6)$$

where  $\hat{g}(\cdot)$  denotes the Fourier transform of window  $g(\cdot)$  and  $\text{supp}(\hat{g}) \in [-\Delta_\omega, \Delta_\omega]$ . It can be known that the STFT of signal (5) is consisted by a series of TF coefficients with the same IP but the distinct IAs. Due to  $\hat{g}(\omega) \leq \hat{g}(0)$ , in the frequency direction, the amplitude of the TF coefficients decreasing with the increasing distance to the IF trajectory. Meanwhile, the IP of the TF coefficients is equivalent to that of the original signal. According to this property, it is first suggested to calculate the derivative of  $G(t, \omega)$  with respect to time,

$$\begin{aligned} \partial_t G(t, \omega) &= \partial_t (A(t)e^{i\varphi(t)} \hat{g}(\omega - \varphi'(t))) \\ &= A(t)e^{i\varphi(t)} \hat{g}(\omega - \varphi'(t)) i\varphi'(t) \\ &= G(t, \omega) i\varphi'(t). \end{aligned} \quad (7)$$

Then, the expression (7) leads to (8): for any  $(t, \omega)$  and for which  $G(t, \omega) \neq 0$ , a 2D IF estimate  $\hat{\omega}(t, \omega)$  for the STFT result (6) can be obtained by

$$\hat{\omega}(t, \omega) = \frac{\partial_t G(t, \omega)}{iG(t, \omega)}. \quad (8)$$

In Ref. [7, 8], it has been proved that, put  $\tilde{\varepsilon} = \varepsilon^{1/3}$ , and assume  $\varepsilon$  being sufficient small, for  $|G(t, \omega)| \geq \tilde{\varepsilon}$ , we have the approximation,

$$|\hat{\omega}(t, \omega) - \varphi'(t)| \leq \tilde{\varepsilon}. \quad (9)$$

The (9) illustrates that, for the weakly time-varying signal (5), the IF estimate  $\hat{\omega}(t, \omega)$  can be well approximated to the signal true IF. The SST employs a frequency reassignment operator to gather the spread TF coefficients, which is expressed as

$$Ts(t, \eta) = \int_{-\infty}^{+\infty} G(t, \omega) \delta(\eta - \hat{\omega}(t, \omega)) d\omega. \quad (10)$$

By the SST operation, the blurry energy of the STFT result can be concentrated in a compact region around the IF trajectories of each mode. Now, we consider the multi-component signal model (2). It is first necessary to assume that each mode can be separated by sufficient distance,

$$\varphi'_k(t) - \varphi'_{k-1}(t) > 2\Delta_\omega \quad (11)$$

where  $k \in \{2, \dots, K\}$ . And then, for the signal (2), the Ref. [7, 8] also proved the following property,

$$\left| (2\pi g(0))^{-1} \int_{|\omega - \varphi'_k(t)| < ds} Ts(t, \omega) d\omega - s_k(t) \right| \leq C\tilde{\varepsilon}. \quad (12)$$

According to (12), each mode can be reconstructed by the TF coefficients around their IF trajectories,

$$s_k(t) \approx (2\pi g(0))^{-1} \int_{|\omega - \varphi'_k(t)| < ds} Ts(t, \omega) d\omega. \quad (13)$$

where  $ds$  denotes the reconstruction bandwidth of the SST. It can be seen that the SST operation not only improves the TF energy-concentration but also retains the signal reconstruction ability.

Furthermore, we consider the cross-terms of the SST representation when addressing multi-component signals. A signal consisting of two modes is first modelled as

$$s(t) = s_1(t) + s_2(t) = A_1(t)e^{i\varphi_1(t)} + A_2(t)e^{i\varphi_2(t)}. \quad (14)$$

Let  $G_k(t, \omega)$  denotes the STFT of the mode  $s_k(t)$ . Assuming that these two modes are weakly time-varying, i.e.,  $|A'_k(t)| \leq \varepsilon$  and  $|\varphi''_k(t)| \leq \varepsilon$  for  $\forall t$ . According to the linearity property of the STFT, we have the expression,

$$G(t, \omega) = G_1(t, \omega) + G_2(t, \omega) = A_1(t)e^{i\varphi_1(t)} \hat{g}(\omega - \varphi'_1(t)) + A_2(t)e^{i\varphi_2(t)} \hat{g}(\omega - \varphi'_2(t)). \quad (15)$$

Then, substituting (15) into (8), we obtain the IF estimate,

$$\hat{\omega}(t, \omega) = \frac{\partial_t (G_1(t, \omega) + G_2(t, \omega))}{i(G_1(t, \omega) + G_2(t, \omega))} \quad (16)$$

Because  $\hat{g}(\omega)$  supports in the region  $[-\Delta_\omega, \Delta_\omega]$ , thus

$$\hat{g}(\omega) \begin{cases} \neq 0 & \text{if } \omega \in [-\Delta_\omega, \Delta_\omega] \\ = 0 & \text{if } \omega \notin [-\Delta_\omega, \Delta_\omega] \end{cases}. \quad (17)$$

If these two modes satisfy the condition (11), i.e.,  $\varphi'_2(t) - \varphi'_1(t) > 2\Delta_\omega$ . According to (7), we can have the following expression,

$$\hat{\omega}(t, \omega) = \begin{cases} \varphi'_1(t), & \text{if } \omega \in [\varphi'_1(t) - \Delta_\omega, \varphi'_1(t) + \Delta_\omega] \\ \varphi'_2(t), & \text{if } \omega \in [\varphi'_2(t) - \Delta_\omega, \varphi'_2(t) + \Delta_\omega] \end{cases} \quad (18)$$

Then, substituting (18) into (10), we can obtain the SST representation as

$$\begin{aligned} (Ts(t, \eta))^2 &= \left( \int_{\varphi'_1(t) - \Delta_\omega}^{\varphi'_1(t) + \Delta_\omega} G_1(t, \omega) \delta(\eta - \varphi'_1(t)) d\omega + \int_{\varphi'_2(t) - \Delta_\omega}^{\varphi'_2(t) + \Delta_\omega} G_2(t, \omega) \delta(\eta - \varphi'_2(t)) d\omega \right)^2 \\ &= 2\pi g(0) \left( A_1(t)^2 \delta(\eta - \varphi'_1(t)) + A_2(t)^2 \delta(\eta - \varphi'_2(t)) + 2A_1(t)A_2(t) \delta(\eta - \varphi'_1(t)) \delta(\eta - \varphi'_2(t)) \right) \end{aligned} \quad (19)$$

where,

$$\int_{\varphi'_k(t) - \Delta_\omega}^{\varphi'_k(t) + \Delta_\omega} G_k(t, \omega) d\omega = \int_{-\infty}^{+\infty} G_k(t, \omega) d\omega = 2\pi g(0) A_k(t) e^{i\varphi_k(t)}. \quad (20)$$

From (19), it is known that, when these two modes are separated with sufficient distances, i.e. satisfying the condition (11), the third term of the expression (19) should be equal to zero. It means that there are not cross-terms in the SST representation. However, the SST representation will produce cross-terms, if these two modes are too close or have cross points, i.e.,

$$|\varphi'_2(t) - \varphi'_1(t)| < 2\Delta_\omega. \quad (21)$$

### B. Multi-synchrosqueezing transform

To generate a concentrated TF representation, the SST requires to be established on the assumption that the analyzed signal should be weakly time-varying. Many studies have shown that, when addressing the strong FM signals, the error between the IF estimate and the true IF will become larger with the increasing signal non-stationarity, which eventually results in a blurry SST representation [12-18]. Although the SST cannot deal with the strongly time-varying signals very well, a factor must be acknowledged that, by using a single SST operation, we can obtain a sharper TF representation than the STFT result at least. In this case, it is motivated to execute another SST operation to the already acquired SST result. Thus, we can obtain a much sharper TF result than the SST result. Then, by iteratively applying multiple SST operations, the energy of the TF result should be concentrated in a step-wise manner. With this idea, we propose the method and formulate it as

$$\begin{aligned} Ts^{[2]}(t, \eta) &= \int_{-\infty}^{+\infty} Ts^{[1]}(t, \omega) \delta(\eta - \hat{\omega}(t, \omega)) d\omega \\ Ts^{[3]}(t, \eta) &= \int_{-\infty}^{+\infty} Ts^{[2]}(t, \omega) \delta(\eta - \hat{\omega}(t, \omega)) d\omega \\ &\vdots \\ Ts^{[N]}(t, \eta) &= \int_{-\infty}^{+\infty} Ts^{[N-1]}(t, \omega) \delta(\eta - \hat{\omega}(t, \omega)) d\omega \end{aligned} \quad (22)$$

where  $Ts(t, \eta)$  in (10) is now denoted by  $Ts^{[1]}(t, \eta)$  and  $N$  is the iteration number such that  $N \geq 2$ . Because (22) executes multiple SST operations to the TF representation iteratively, we name this method multi-synchrosqueezing transform (MSST). Then, we will provide the detailed mathematical analysis to show its effectiveness in concentrating TF energy. Considering that the MSST employs an iterative procedure to address the TF representation, the main focus is first on the comparison between the MSST ( $N=2$ ) and the original SST. We substitute  $Ts^{[1]}(t, \eta)$  into  $Ts^{[2]}(t, \eta)$ , and then the MSST ( $N=2$ ) can be expressed as

$$\begin{aligned} Ts^{[2]}(t, \eta) &= \int_{-\infty}^{+\infty} Ts^{[1]}(t, \xi) \delta(\eta - \hat{\omega}(t, \xi)) d\xi \\ &= \int_{-\infty}^{+\infty} \int_{-\infty}^{+\infty} G(t, \omega) \delta(\xi - \hat{\omega}(t, \omega)) d\omega \delta(\eta - \hat{\omega}(t, \xi)) d\xi \\ &= \int_{-\infty}^{+\infty} G(t, \omega) \int_{-\infty}^{+\infty} \delta(\xi - \hat{\omega}(t, \omega)) \delta(\eta - \hat{\omega}(t, \xi)) d\xi d\omega \\ &= \int_{-\infty}^{+\infty} G(t, \omega) \delta(\eta - \hat{\omega}(t, \hat{\omega}(t, \omega))) d\omega. \end{aligned} \quad (23)$$

From (23), it can be known that the MSST ( $N=2$ ) constructs a novel IF estimate  $\hat{\omega}(t, \hat{\omega}(t, \omega))$  to reassign the blurry STFT result, and then we will prove that this novel IF estimate is more suitable for addressing strong FM signals than the  $\hat{\omega}(t, \omega)$ . Herein, a more general assumption is first given that  $\exists \varepsilon$  sufficient small,  $|A'(t)| \leq \varepsilon$  and  $|\varphi'''(t)| \leq \varepsilon$  for  $\forall t$ , such that the signal (4) can be approximately regarded as the linear chirp signal in a short time. According to the Taylor expansion, we can expand the  $A(u)$  and  $\varphi(u)$  at the time point  $t$ . The related

expressions are written as, respectively,  $A(u) = A(t)$  and  $\varphi(u) = \varphi(t) + \varphi'(t)(u-t) + 0.5\varphi''(t)(u-t)^2$ , where the terms on the order  $O(A'(t))$  and  $O(\varphi'''(t))$  are neglected. Therefore, the signal (4) can be rewritten as

$$s(u) = A(t)e^{i(\varphi(t) + \varphi'(t)(u-t) + 0.5\varphi''(t)(u-t)^2)}. \quad (24)$$

Meanwhile, we specify the window function as Gaussian function  $g(t) = e^{-0.5t^2}$ , and then the STFT of signal (24) can be derived that,

$$\begin{aligned} G(t, \omega) &= \int_{-\infty}^{+\infty} e^{-0.5(u-t)^2} A(t)e^{i(\varphi(t) + \varphi'(t)(u-t) + 0.5\varphi''(t)(u-t)^2)} e^{-i\omega(u-t)} du \\ &= A(t)e^{i\varphi(t)} \int_{-\infty}^{+\infty} e^{-0.5(1-i\varphi''(t))(u-t)^2} e^{-i(\omega-\varphi'(t))(u-t)} d(u-t) \\ &= A(t)e^{i\varphi(t)} \frac{1}{\sqrt{1-i\varphi''(t)}} e^{-\frac{(\omega-\varphi'(t))^2}{2(1-i\varphi''(t))}}. \end{aligned} \quad (25)$$

Then, substituting (25) into (8), the 2D IF estimate of signal (24) can be obtained,

$$\begin{aligned} \hat{\omega}(t, \omega) &= \varphi'(t) + \frac{\varphi''(t)^2}{1 + \varphi''(t)^2} (\omega - \varphi'(t)) - i \frac{\varphi''(t)}{1 + \varphi''(t)^2} (\omega - \varphi'(t)). \end{aligned} \quad (26)$$

Because the (26) is a complex value, which cannot be directly used for calculation. Therefore, in Ref. [7-9, 14-19], they suggest to take the real part of (26) as the IF estimate, and then the (26) should be rewritten as

$$\hat{\omega}(t, \omega) = \varphi'(t) + \frac{\varphi''(t)^2}{1 + \varphi''(t)^2} (\omega - \varphi'(t)). \quad (27)$$

It can be seen that the  $\hat{\omega}(t, \omega)$  cannot provide an unbiased estimate for the true IF of the signal (24). The error between  $\hat{\omega}(t, \omega)$  and  $\varphi'(t)$  i.e.,  $|\hat{\omega}(t, \omega) - \varphi'(t)|$ , depends on two factors, respectively, the second-order derivative of IP and the distance between frequency variable and true IF. For the strong FM signals, the item  $\varphi''(t)$  cannot be neglected, which lead to that the  $|\hat{\omega}(t, \omega) - \varphi'(t)|$  becomes larger and larger with the increasing distance between frequency variable and true IF. It is the reason that the original SST cannot generate a concentrated TF representation for strongly time-varying signals.

According to (27), we can further obtain the IF estimate of the MSST (N=2) as

$$\begin{aligned} \hat{\omega}(t, \hat{\omega}(t, \omega)) &= \varphi'(t) + \frac{\varphi''(t)^2}{1 + \varphi''(t)^2} (\hat{\omega}(t, \omega) - \varphi'(t)) \\ &= \varphi'(t) + \left( \frac{\varphi''(t)^2}{1 + \varphi''(t)^2} \right)^2 (\omega - \varphi'(t)). \end{aligned} \quad (28)$$

Furthermore, we can derive that

$$\begin{aligned} |\hat{\omega}(t, \hat{\omega}(t, \omega)) - \varphi'(t)| &= \left| \frac{\varphi''(t)^2}{1 + \varphi''(t)^2} (\hat{\omega}(t, \omega) - \varphi'(t)) \right| \\ &< |(\hat{\omega}(t, \omega) - \varphi'(t))|. \end{aligned} \quad (29)$$

The (29) illustrates that the  $\hat{\omega}(t, \hat{\omega}(t, \omega))$  is much closer to the signal true IF than the  $\hat{\omega}(t, \omega)$ , which lead to the MSST (N=2) can provide the more concentrated result than the

original SST. From the viewpoint of the geometry reassignment, the differences between SST and the MSST (N=2) are further demonstrated in Fig. 1. As shown in Fig. 1(a), it is assumed that the  $(t, \omega)$  is an arbitrary point in the TF plane, which corresponds to the TF coefficient  $G(t, \omega)$ . The SST is to reassign the TF coefficient from  $(t, \omega)$  to the newly calculated point  $(t, \hat{\omega}(t, \omega))$ . The IF trajectory of a purely harmonic signal should be a straight line that is parallel to the time axis. Because the IF estimate of STFT result for harmonic signal is equal to the signal IF, i.e.,  $\hat{\omega}(t, \omega) = \varphi'(t)$ , the SST operation can effectively reassign the TF coefficient from the point  $(t, \omega)$  to the IF trajectory  $(t, \varphi'(t))$ . According to the (27), it is known that the  $\hat{\omega}(t, \omega)$  is a biased estimate for the strongly time-varying signal IF. Therefore, only single SST operation cannot provide enough distance to reassign the TF coefficient to the IF trajectory, as shown in Fig. 1(b). Compared with the SST, the MSST (N=2) executes one more reassignment for the TF coefficient  $Ts(t, \omega)$  from the point  $(t, \hat{\omega}(t, \omega))$  to the point  $(t, \hat{\omega}(t, \hat{\omega}(t, \omega)))$ . Because the IF estimate  $\hat{\omega}(t, \hat{\omega}(t, \omega))$  is much closer to the time-varying signal IF, the MSST (N=2) can provide more concentrated TF representation than the SST.

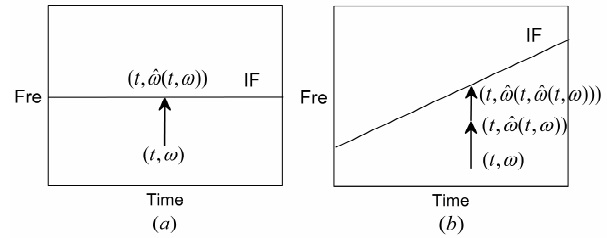


Fig. 1 (a) Reassignment manner of the SST and (b) reassignment manner of the MSST.

If we substitute  $Ts^{[2]}(t, \eta)$  into  $Ts^{[3]}(t, \eta)$ , the MSST (N=3) can be derived that,

$$\begin{aligned} Ts^{[3]}(t, \eta) &= \int_{-\infty}^{+\infty} Ts^{[2]}(t, \xi) \delta(\eta - \hat{\omega}(t, \xi)) d\xi \\ &= \int_{-\infty}^{+\infty} G(t, \omega) \delta(\xi - \hat{\omega}(t, \hat{\omega}(t, \omega))) d\omega \delta(\eta - \hat{\omega}(t, \xi)) d\xi \\ &= \int_{-\infty}^{+\infty} G(t, \omega) \int_{-\infty}^{+\infty} \delta(\xi - \hat{\omega}(t, \hat{\omega}(t, \omega))) \delta(\eta - \hat{\omega}(t, \xi)) d\xi d\omega \\ &= \int_{-\infty}^{+\infty} G(t, \omega) \delta(\eta - \hat{\omega}(t, \hat{\omega}(t, \hat{\omega}(t, \omega)))) d\omega. \end{aligned} \quad (30)$$

It can be seen that, the MSST (N=3) construct a novel IF estimate  $\hat{\omega}(t, \hat{\omega}(t, \hat{\omega}(t, \omega)))$ . If we further substitute  $Ts^{[N-1]}(t, \eta)$  into  $Ts^{[N]}(t, \eta)$ , we can calculate the IF estimate of the MSST with more iterations, for instance,  $\hat{\omega}(t, \hat{\omega}(t, \hat{\omega}(t, \hat{\omega}(t, \hat{\omega}(t, \omega)))))$  is the IF estimate of MSST (N=4),  $\hat{\omega}(t, \hat{\omega}(t, \hat{\omega}(t, \hat{\omega}(t, \hat{\omega}(t, \hat{\omega}(t, \omega)))))$  is the IF estimate of MSST (N=5), and so on. Therefore, we let  $\hat{\omega}^{[N]}(t, \omega)$  denote the IF estimate of MSST, and then can rewrite the expression of the MSST as

$$Ts^{[N]}(t, \eta) = \int_{-\infty}^{+\infty} G(t, \omega) \delta(\eta - \hat{\omega}^{[N]}(t, \omega)) d\omega. \quad (31)$$

Moreover, according to (27), the corresponding IF estimate of the MSST can also be calculated as

$$\hat{\omega}^{[N]}(t, \omega) = \varphi'(t) + \left( \frac{\varphi''(t)^2}{1 + \varphi''(t)^2} \right)^N (\omega - \varphi'(t)). \quad (32)$$

It can be known that, by each iteration, the MSST will construct a novel IF estimate to reassign the blurry STFT energy. It is obvious that, by multiple iterations, the IF estimate of the MSST method will be closer and closer to the signal true IF. Therefore, the energy of the TF representation can be concentrated in a stepwise manner.

### C. Algorithm implementation

In this section, we mainly consider the algorithm implementation of the discrete MSST. The expressions (22) and (31) correspond to two distinct implementation way of the MSST, respectively. The expression (22) is straight and easy to implement just by executing multiple SST operations. However, according to the research in [7, 8], the SST operation is a little bit time-consuming. The multiple SST operations will bring significantly computational burden, which heavily hinders the real-time application of MSST in practical engineering. However, the expression (31) inspires that, we can first construct the IF estimate  $\hat{\omega}^{[N]}(t, \omega)$  of the MSST by employing the function iteration, and then execute once SST operation to reassign the STFT result. This implementation way can highly decrease the computational burden, because it only needs to execute once SST operation.

For the discrete data  $s[l]$ ,  $l=0,1,\dots,L-1$ , where  $L$  is the number of samples, and the data  $s[l]$  correspond to a uniform discretization of  $s(t)$  taken at the time  $t_n = t_0 + lT$ , where  $T$  is the sampling interval. The Fourier transform of data  $s[l]$  is calculated by  $S[m] = \sum_{l=0}^{L-1} s[l] e^{-i\frac{2\pi}{L}lm}$ , where  $m=0,1,\dots,L-1$ .

Meanwhile, the discrete STFT is written as

$$G[h, m] = \sum_{l=0}^{L-1} s[l] g[l-h] e^{-i\frac{2\pi}{N}m[l-h]}. \quad (33)$$

Then, we can obtain the discrete IF estimate,

$$\hat{\omega}[h, m] = \begin{cases} \text{Ro} \left[ \text{Re} \left[ \frac{N}{2\pi i} \ln \left[ \frac{G[h+1, m]}{G[h, m]} \right] \right] \right], & \text{if } G[h, m] \neq 0 \\ 0, & \text{if } G[h, m] = 0 \end{cases}. \quad (34)$$

where  $\text{Ro}[\cdot]$  denotes the round operation and  $\text{Re}[\cdot]$  denotes taking real part. Then, the discrete SST should be written as

$$Ts[h, \xi] = \sum_{m=0}^{L-1} G[h, m] \delta[\xi - \hat{\omega}[h, m]]. \quad (35)$$

Therefore, the discrete version of the expression (22) can be written as

$$\begin{aligned} Ts^{[2]}[h, \xi] &= \sum_{m=0}^{L-1} Ts^{[1]}[h, m] \delta[\xi - \hat{\omega}[h, m]] \\ Ts^{[3]}[h, \xi] &= \sum_{m=0}^{L-1} Ts^{[2]}[h, m] \delta[\xi - \hat{\omega}[h, m]] \\ &\vdots \\ Ts^{[N]}[h, \xi] &= \sum_{m=0}^{L-1} Ts^{[N-1]}[h, m] \delta[\xi - \hat{\omega}[h, m]] \end{aligned} \quad (36)$$

Meanwhile, the discrete (31) can be written as

$$Ts^{[N]}[h, \xi] = \sum_{m=0}^{L-1} G[h, m] \delta[\xi - \hat{\omega}^{[N]}[h, m]] \quad (37)$$

The Pseudocode of expressions (36) and (37) can be found in Algorithm 1 and Algorithm 2, respectively. In which,  $h$  denotes the discrete time variable,  $m$  and  $\xi$  denote the discrete frequency variable.

---

#### Algorithm 1 Expression (22)-based MSST

---

##### Step 1: Initialization and Calculation

Choose the window function  $g$  and iteration number  $N$ ;  
Calculate STFT  $G[h, m]$  and IF estimate  $\hat{\omega}[h, m]$ ;

##### Step 2: Multi-Synchrosqueezing

$Ts^{[1]}[h, \xi] \leftarrow 0$ ;

$Ts^{[0]}[h, m] \leftarrow G[h, m]$ ;

**for**  $n = 1 : N$

**for**  $h = 1 : L$

**for**  $m = 1 : L$

$\xi \leftarrow \hat{\omega}[h, m]$ ;

$Ts^{[n]}[h, \xi] \leftarrow Ts^{[n]}[h, \xi] + Ts^{[n-1]}[h, m]$ ;

**end for**

**end for**

**end for**

**output**  $Ts^{[N]}[h, \xi]$

---



---

#### Algorithm 2 Expression (31)-based MSST

---

##### Step 1: Initialization and Calculation

Choose the window function  $g$  and iteration number  $N$ ;  
Calculate STFT  $G[h, m]$  and IF estimate  $\hat{\omega}[h, m]$ ;

##### Step 2: Construct IF estimate of MSST

$\hat{\omega}^{[1]}[h, m] \leftarrow \hat{\omega}[h, m]$

**if**  $N > 1$

**for**  $n = 2 : N$

**for**  $h = 1 : L$

**for**  $m = 1 : L$

$\xi \leftarrow \hat{\omega}^{[n-1]}[h, m]$ ;

$\hat{\omega}^{[n]}[h, m] \leftarrow \hat{\omega}^{[n-1]}[h, \xi]$ ;

**end for**

**end for**

**end for**

**end if**

##### Step 3: Synchrosqueezing

$Ts^{[N]}[h, \xi] \leftarrow 0$ ;

**for**  $h = 1 : L$

**for**  $m = 1 : L$

$\xi \leftarrow \hat{\omega}^{[N]}[h, m]$ ;

$Ts^{[N]}[h, \xi] \leftarrow Ts^{[N]}[h, \xi] + G[h, m]$ ;

**end for**

**end for**

**output**  $Ts^{[N]}[h, \xi]$

---

It can be seen that, the Algorithm 1 and Algorithm 2 mainly lie into two steps and three steps, respectively. In theory, the integral operation in SST is completed by the addition operation in addressing discrete signals. The Algorithm 1 has to execute multiple SST operations in the Step 2, which can bring significantly computational burden when the iteration number is large. In Algorithm 2, it first constructs the novel IF estimate by employing the substitution operation in the Step 2. Eventually, the Algorithm 2 only executes once SST operation, which is obviously less time consuming than the Algorithm 1. Therefore, we suggest implementing the MSST with the Algorithm 2.

#### D. Signal reconstruction and ridge detection

Considering that the MSST reassigns the TF coefficients only in the frequency direction and there is no information missing, the MSST should allow for the perfect signal reconstruction in theory. To prove this, we begin with the following expression,

$$\begin{aligned}
 \int_{-\infty}^{+\infty} Ts^{[N]}(t, \eta) d\eta &= \int_{-\infty}^{+\infty} \int_{-\infty}^{+\infty} Ts^{[N-1]}(t, \omega) \delta(\eta - \hat{\omega}(t, \omega)) d\omega d\eta \\
 &= \int_{-\infty}^{+\infty} Ts^{[N-1]}(t, \omega) \int_{-\infty}^{+\infty} \delta(\eta - \hat{\omega}(t, \omega)) d\eta d\omega \\
 &= \int_{-\infty}^{+\infty} Ts^{[N-1]}(t, \omega) d\omega \\
 &\vdots \\
 &= \int_{-\infty}^{+\infty} G(t, \xi) d\xi \\
 &= \int_{-\infty}^{+\infty} \int_{-\infty}^{+\infty} g(u-t) s(u) e^{-i\xi(u-t)} du d\xi \\
 &= 2\pi \int_{-\infty}^{+\infty} g(u-t) s(u) \delta(u-t) du \\
 &= 2\pi g(0) s(t).
 \end{aligned} \tag{38}$$

The (38) illustrates that the original signal can be perfectly recovered via

$$s(t) = (2\pi g(0))^{-1} \int_{-\infty}^{+\infty} Ts^{[N]}(t, \omega) d\omega. \tag{39}$$

Because the MSST result has the more concentrated TF representation than the SST result, each mode also admits the following mode decomposition expression,

$$s_k(t) \approx (2\pi g(0))^{-1} \int_{|\omega - \phi_k(t)| < ds'} Ts^{[N]}(t, \omega) d\omega. \tag{40}$$

where  $ds'$  denotes the reconstruction bandwidth of the MSST. According to (40), to decompose a mode from the MSST result, it requires the precise IF trajectory of the mode. The method described in [22] provides an effective algorithm to detect IF trajectory, which is written as

$$\begin{aligned}
 E(\phi) &= \\
 &\sum_{k=1}^K \int_{-\infty}^{+\infty} |TFR(t, \phi_k(t))|^2 dt - \int_{-\infty}^{+\infty} (\lambda \cdot \phi_k'(t)^2 + \beta \cdot \phi_k''(t)^2) dt
 \end{aligned} \tag{41}$$

where  $\sum_{k=1}^K (t, \phi_k(t))$  is the estimation of the IF trajectories in the

TF plane, and  $\lambda$   $\beta$  are two parameters to adjust the level of regularization. The (41) suggests that both the energy of TF coefficients and the local smoothness of the detected trajectory should be considered. The practical implementation of the IF

detection method in [23] starts from the maximum value in each time point of the TF representation, and then employs the forward and backward procedures to search the local maximum value along the entire TF plane. For the data with large samples, this method will bring heavy computational burden. The algorithm in [24] suggests that the starting point can be selected by the global maximum value of the TF representation, which can obviously decrease the computational cost. However, it cannot guarantee that the global maximum value precisely locates in the true IF trajectory in some cases, which may deviate the original intention of the (41). For instance, the large fluctuation caused by abnormal event or the heavy background noise in the signal may lead to the incorrect starting point. To improve both the efficiency and reliability of the IF detection procedure, the entire TF plane is suggested to be first separated into several segments. The starting point is determined from these individual TF segments instead of from global value. Then the forward and backward procedures are executed to search the IF trajectories, respectively. Eventually, the best IF trajectory is selected from these trajectories according to the TF energy. Given the TF representation  $Ts[h, m]$ , it is separated into  $F$  segments and there are  $K$  modes needed to be detected. The entire ridge detection algorithm combining with the mono-component mode reconstruction can be found in Algorithm 3. In which, the parameter  $\Delta$  is the maximum allowable frequency variation.

---

#### Algorithm 3 mono-component mode decomposition

---

**Input** :  $\Delta, K, F, ds', Ts[h, m]$

**for**  $k = 1$  **to**  $K$

**for**  $f = 1$  **to**  $F$

$$(h', m') \leftarrow \arg \max_{h, m} |Ts[h, m]|, \quad h \in [(f-1)\frac{L}{F}, (f)\frac{L}{F}];$$

$$IF_{k,f}(h') \leftarrow m', \quad IF_{k,f}(h'-1) \leftarrow \arg \max_m |Ts[h'-1, m]|;$$

**for**  $h = h' + 1$  **to**  $L - 1$

$$\begin{aligned}
 IF_{k,f}(h) \leftarrow &\arg \max_{m \in [IF_{k,f}(h-1) - \Delta, IF_{k,f}(h-1) + \Delta]} (|Ts[h, m]|^2 \\
 &- \beta(m - 2IF_{k,g}(h-1) + IF_{k,g}(h-2))^2);
 \end{aligned}$$

**end for**

**for**  $h = h' - 1$  **to**  $0$

$$\begin{aligned}
 IF_{k,f}(h) \leftarrow &\arg \max_{m \in [IF_{k,f}(h+1) - \Delta, IF_{k,f}(h+1) + \Delta]} (|Ts[h, m]|^2 \\
 &- \beta(m - 2IF_{k,f}(h+1) + IF_{k,f}(h+2))^2);
 \end{aligned}$$

**end for**

**end for**

$$IF_k \leftarrow \arg \max_{IF_{k,f}} \sum_{h=0}^{L-1} |Ts[h, IF_{k,f}(h)]|;$$

$$s_k[h] = (2\pi g(0))^{-1} \sum_{m \in [IF_k(h) - ds', IF_k(h) + ds']} Ts[h, m];$$

$$Ts_{m \in [IF_k(h) - \Delta, IF_k(h) + \Delta]}[h, m] \leftarrow 0;$$

**end for**

**Output**:  $\sum_{k=1}^K s_k[h]$

---

### III. NUMERICAL VALIDATION

In this section, we focus on the comparisons between the proposed method and other advanced TFA methods in addressing complex signals, for instance, noisy signals, multi-component signals with closely separated modes and strongly time-varying signals. The comparisons mainly focus on the TF energy concentration, TF resolution, signal reconstruction and computational time.

#### A. Numerical signal with noise

Herein, a numerical signal consisting of two components with distinct IFs is modelled as

$$S(t) = \underbrace{\sin(2\pi(40t + \sin(1.5t)))}_{S1} + \underbrace{\sin(2\pi(17t + 6\sin(1.5t)))}_{S2} \quad (42)$$

where the mode S2 has stronger FM law than the mode S1. For this numerical signal, we add the white noise to it, where the SNR (signal to noise ratio) is equivalent to 12 dB. The TF representations generated by SST and MSST are shown in Fig. 2(a-d), and the local zoom of mode S2 follows in the right side. It can be seen that, in the SST result, the TF features of weak FM mode S1 is as blurry as that of the strong FM mode S2. This is because the added noise decreases the IF estimate accuracy of the SST, even for the weakly time-varying component. However, the MSST still provides the concentrated TF result for these two modes.

For more comparisons, the TF representations generated by second-order SST, forth-order SST, RM and DSST are shown in Fig. 2(e-l). The second-order SST and forth-order SST are established on the more accuracy IF estimate and the TF results are shown in Fig. 2(e-h). However, the high-order SST does not generate the significantly concentrated results. It can be observed that the forth-order SST even generates worse TF results than second-order SST, which means that the high-order IF estimate does not have a good noise robustness. The RM technique is to reassign the spectrogram from TF direction, which results into the concentrated image (Fig. 2(i-j)) than the SST. For the DSST result in Fig. 2(k-l), we employ the extra parameter to demodulate the mode S1. Although the TF features of mode S1 is highly concentrated, the mode S2 appears to be heavily blurry. That is because the selected parameter can only demodulate the specified mode, and the TF feature of the mode with the distinct FM trend is even worse than the SST result.

To display the TF energy distribution more clearly, we plot two TF slices at time  $t=3.3$  s in Fig. 3, which focus on the frequency band around mode S1 and mode S2, respectively. For the reassigned techniques, the better ability of concentrating TF coefficient can generate the TF result with narrower energy distribution and larger TF amplitude. For instance, the SST is not suitable for addressing strongly time-varying mode. It can be seen that the SST result of mode S2 has larger energy distribution and lower amplitude than that of mode S1. The second-order SST and forth-order SST have the same performance in addressing noisy signal. The DSST provides a more significantly concentrated TF slice for mode S1 than mode S2. It is because we utilize the extra parameter to demodulate the mode S1. Because the MSST has the best

ability of concentrating TF coefficients than other reassigned techniques, the corresponding TF slices of modes S1 and S2 have the narrowest frequency band and the largest TF energy. It can be concluded that, the MSST is more suitable for addressing time-varying signal with noise than other TFA methods.

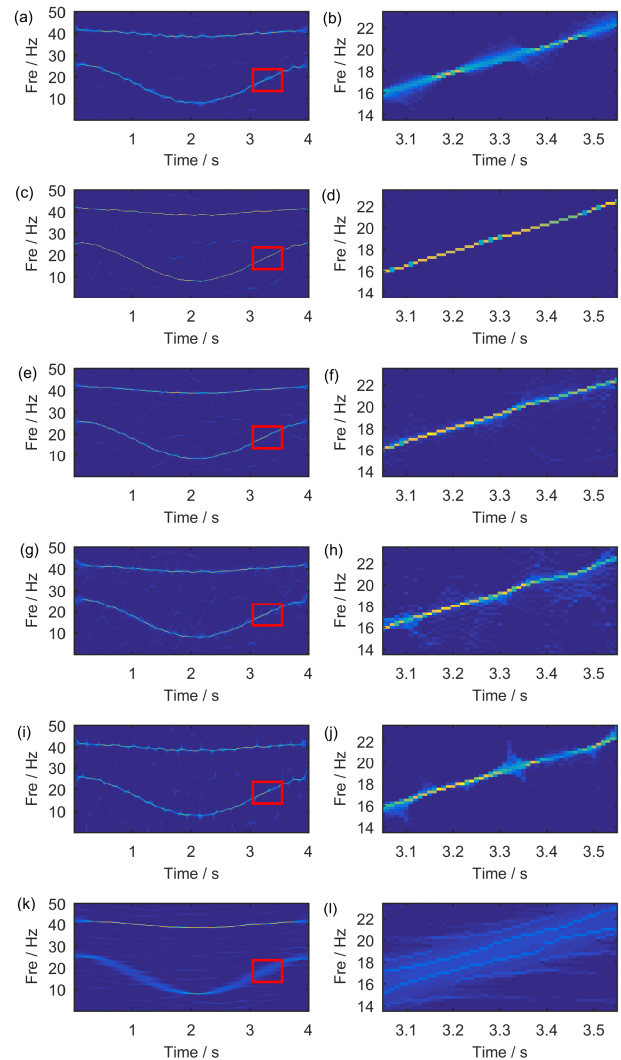


Fig. 2 (a) SST result, (b) local zoom on SST result, (c) MSST result and (d) local zoom on MSST result, (e) second-SST result, (f) local zoom on second-SST result, (g) forth-order SST result, (h) local zoom on forth-order SST result, (i) RM result, (j) local zoom on RM result, (k) DSST result and (l) local zoom on DSST result.

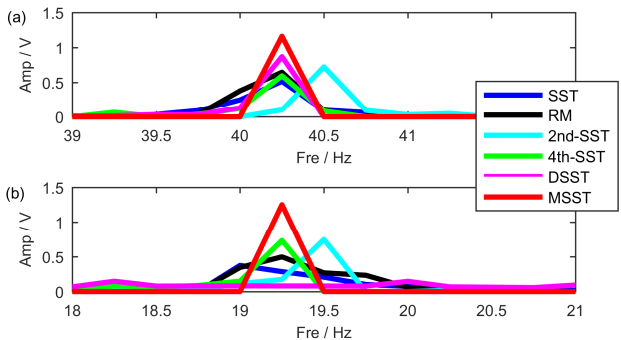


Fig. 3 (a) The TF slices of (a) mode S1 and (b) mode S2 at time  $t=3.3$  s.

For more comparisons, we provide the quadratic time-frequency distribution (QTFD) results. In Fig. 4, these TF results are generated by Wigner-Ville distribution (WVD), pseudo WVD (PWVD), reduced-interference distribution with triangular kernel (RIDT) and reduced-interference distribution with Hanning kernel (RIDH), respectively. It can be seen that, affected by the heavy cross-terms, the WVD fails to provide useful information for the signal. Although the PWVD roughly characterizes the time-varying features of two modes, it also produces unexpected cross-terms. The RIDT and RIDH generate similar TF results without obvious cross-terms. However, these two representations have much larger TF energy distribution than the SST techniques.

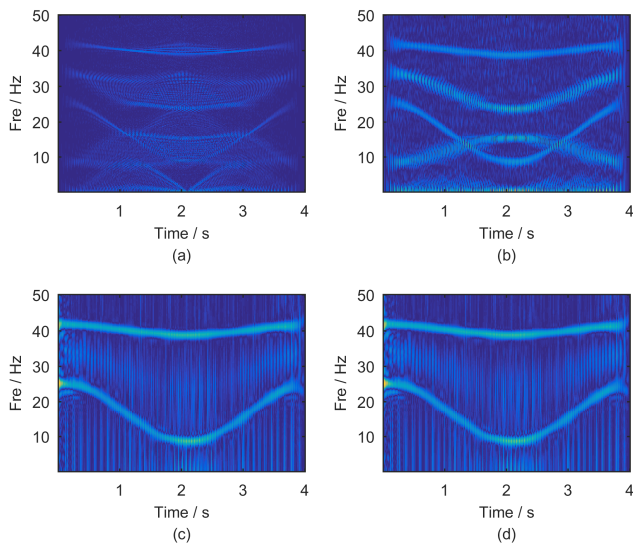


Fig. 4 (a) WVD result, (b) PWVD result, (c) RIDT result and (d) RIDH result.

Furthermore, to evaluate the energy concentration of different TFA methods quantitatively, we calculate the Rényi entropies of these TF results and list them in Table I, where a lower Rényi entropy value denotes a more concentrated TF representation. It is shown that the reassigned techniques can provide more concentrated result than the QTFD methods. In which, the MSST obviously provides the most concentrated result among all TFA methods.

TABLE I  
RÉNYI ENTROPY BY SEVERAL TFA METHODS

TFA	SST	MSST	RM	2nd-SST	4th-SST
<b>Rényi Entropy</b>	11.3117	9.9448	11.222	11.1565	11.5984
TFA	DSST	WVD	PWVD	RIDT	RIDH
<b>Rényi Entropy</b>	11.7265	14.8095	14.6968	14.7741	14.7728

To decompose these two modes, we first detect the IF trajectories, which are shown in Fig. 5. The decomposition results are shown in Fig. 6. It can be found that, although both of two methods can decompose these two modes, the decomposed results of the MSST are much closer to the original signal than that of the SST. It is because the blurry energy of SST representation results in that the TF coefficients belonging to these two modes cannot be enough integrated in a compact region. However, if we consider large integration region to reconstruct these two modes, it may introduce more unexpected noise. Furthermore, we calculate the SNR values of

two reconstructed modes compared to the numerical signal, which are 10.2959 dB (mode S1 by SST), 8.9485 dB (mode S2 by SST), 14.7645 dB (mode S1 by MSST) and 14.3621 dB (mode S2 by MSST), respectively. It can be seen that the SNR value of the SST-recovered mode S1 is larger than that of the SST-recovered mode S2, which means that the SST performs worse reconstruction for strongly time-varying mode. However, both of two MSST-recovered modes have large SNR values. Therefore, it can be concluded that the energy-concentrated TFA method is more suitable for mono-component mode decomposition.

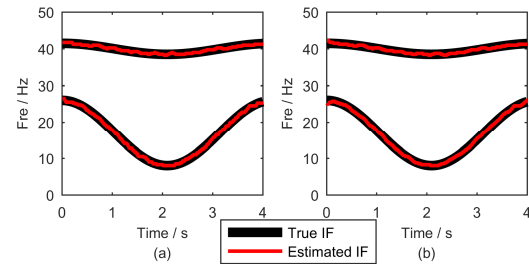


Fig. 5 (a) SST-based IF Detection result, (b) MSST-based IF Detection result.

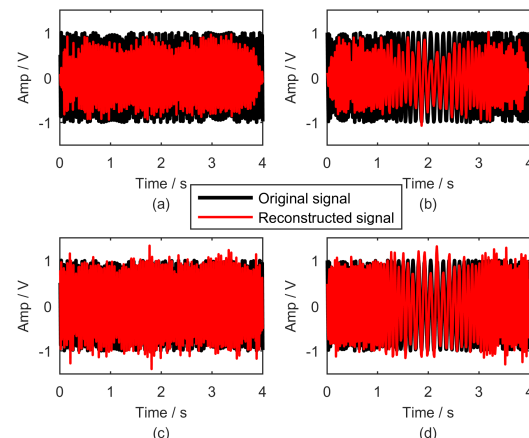


Fig. 6 (a) Mode S1 and (b) mode S2 reconstructed by SST result, (c) mode S1 and (d) mode S2 reconstructed by MSST result.

Moreover, we test the reconstruction performance of the MSST with respect to iteration number. The analysis results are evaluated by the SNR of the superposition of two reconstructed modes, which are shown in Fig. 7. It can be seen that more iterations can lead to higher SNR reconstructed results. After six iterations, the SNR indicates to be stable.

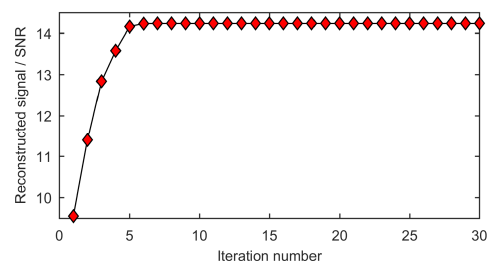


Fig. 7 SNR of the reconstructed results with respect to iteration number

The efficiency of a TFA method is essential in real-time applications, which decides whether or not the method can be used in practical engineering. Herein, we test the computational time required for the above-mentioned TFA methods in addressing this noisy signal. The tested computer configuration

is as follows: Intel Core i7-6500 2.5 GHz, 8.0 GB of DDR3 RAM, Windows 10 OS, and MATLAB version R2016a. The required computation times are listed in Table II. It can be seen that, all methods can finish the processing within one second. With the increase of the iteration number, the calculation time of the MSST method does not increase significantly. Although we select large iteration number, the computational time of the MSST method is still less than the high-order SST methods.

TABLE II  
REQUIRED COMPUTATIONAL TIME BY SEVERAL TFA METHODS

TFA	SST	2nd-SST	3rd-SST	4th-SST
Time (s)	0.07	0.12	0.23	0.33
TFA	RM	MSST (N=6)	MSST (N=30)	MSST (N=100)
Time (s)	0.075	0.071	0.095	0.21

**B. Strongly time-varying signal**

In this section, we consider a strongly time-varying signal to analyze, which is borrowed from Ref. [16]. The signal is modelled as

$$S(t) = \underbrace{\sin(2\pi(340t - 2 \exp(-2t + 0.4) \sin(14\pi(t - 0.2))))}_{S1} + \underbrace{\sin(2\pi(75t + 30t^3))}_{S2} \quad (43)$$

where the mode S1 is strongly time-varying and the mode S2 is weakly time-varying.

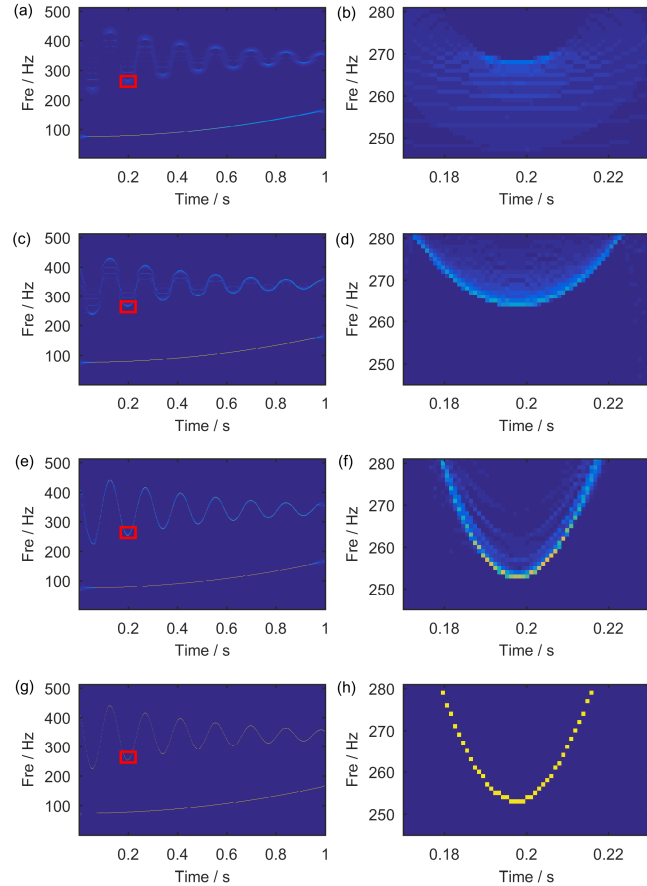


Fig. 8 (a) SST result, (b) local zoom on SST result, (c) second-SST result, (d) local zoom on second-SST result, (e) forth-order SST result, (f) local zoom on forth-order SST result (g) MSST result and (h) local zoom on MSST result.

The focus is on the TF energy distribution of the proposed method and high-order SST methods in addressing the mode S1 of this noise-free signal. The TF representations and the TF slices are displayed in Fig. 8 and Fig. 9, respectively. It can be observed that, for mode S2, all methods can provide an energy-concentrated result. However, for mode S1, the SST result smears heavily. With the increase of the SST order, the TF energy becomes more and more concentrated. From the TF slice and the local zoom on TF result of mode S1, it is obvious that, the MSST result is the most concentrated.

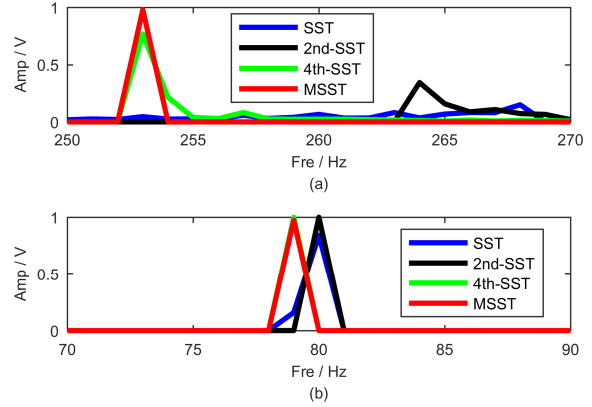


Fig. 9 The TF slices of (a) mode S1 and (b) mode S2 at time  $t=0.2$  s.

**C. Closely-separated multi-component signal**

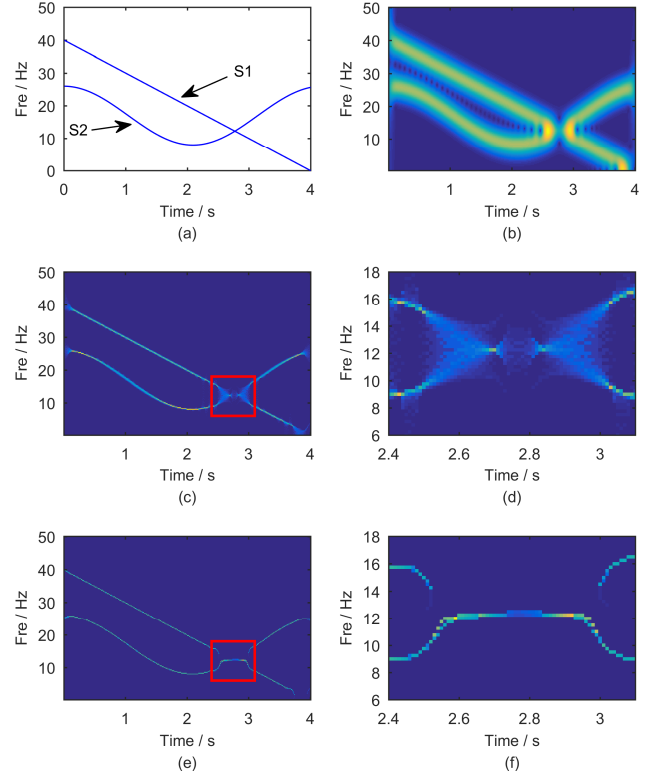


Fig. 10 (a) True IF, (b) STFT result, (c) SST result, (d) local zoom on SST result, (e) MSST result and (f) local zoom on MSST result.

In this section, we consider a numerical signal to test the performance of the proposed method in addressing closely separated multi-component signal. The signal is modelled as

$$S(t) = \underbrace{\sin(2\pi(40t - 5t^2))}_{S_1} + \underbrace{\sin(2\pi(17t + 6\sin(1.5t)))}_{S_2} \quad (44)$$

where two modes have the cross point at the time 2.7 s. The true IF is plotted in Fig. 10(a). And then the STFT result, SST result, MSST result and their local features are displayed in Fig. 10(b-f). It can be observed that, for the SST result, in the TF plane around the cross point, there are heavy cross-terms between two modes. Although the MSST result appears to be more concentrated, the corresponding TF result cannot characterize the true IF trajectories. Therefore, the SST-based techniques is more suitable for addressing the signals that can satisfy the well-separated condition (11).

#### IV. EXPERIMENTAL VALIDATION

In this section, we mainly consider the applications of the proposed method in addressing real-world signals. We select two practical signals to show the effectiveness of the MSST by comparing with other TFA methods.

##### A. Rotating machinery early rub-impact fault vibration signal analysis

In this section, we focus on an abnormal vibration of a heavy oil catalytic machine set [2, 25]. The structural sketch is shown in Fig. 11. The bearing cases (1#, 2#, 3# and 4#) are used to support the corresponding shaft. The vibration sensors are mounted on the bearing cases with a sampling frequency of 2 kHz. It has been known that the vibration in bearing 2# is larger than the alarm limitation, which is due to the existence of a rub-impact fault between the rotor and the static element. The main focus is on the instantaneous TF features of the signal recorded from the bearing 2#. The rotation speed of the gas turbo is 5381 rpm (where the rotating frequency is approximately equal to 90 Hz).

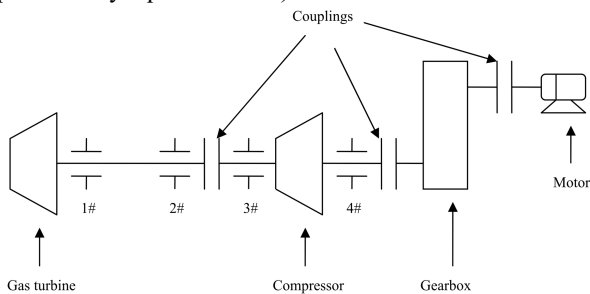


Fig. 11. The structural sketch of the machine set.

The waveform of the vibration signal and its spectrum are shown in Fig. 12. It can be seen that the first-order rotating frequency is the largest component, which corresponds to the main fault reason. However, the main concern should not only be the largest component, but also pay much attention on the weak components. It is because the weak components may contain more essential information being closely related to the early fault features. To enhance the TF features of weak components, we display the logarithm of the MSST analysis result (see Fig. 13). It can be clearly observed that three modes M1, M2 and M3 and their oscillated TF features are characterized. Then the ridge detection algorithm is used to estimate the IFs of three modes, which are displayed in Figs.

14-16, meanwhile the spectrum follows to further reveal the oscillated frequency of the IF trajectory.

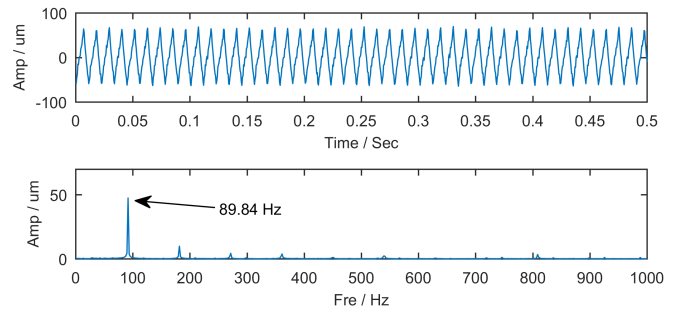


Fig. 12. The waveform of the vibration signal and its spectrum.

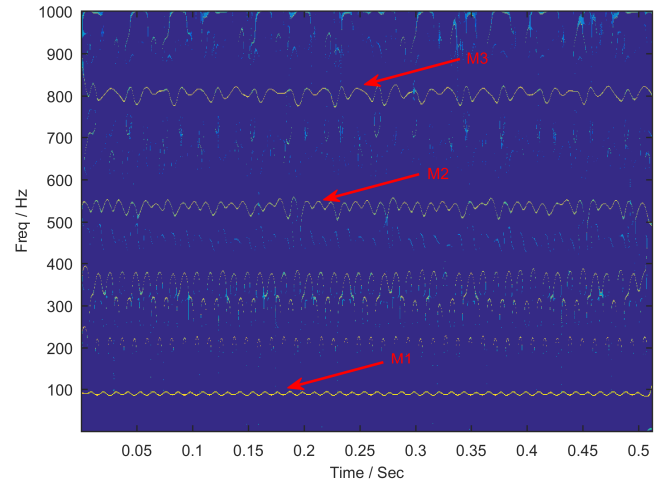


Fig. 13. The logarithm of the MSST analysis result.

Fig. 14 shows that the IF of mode M1 periodically oscillates around first-order rotating frequency with the frequency of 89.94 Hz. This is because the rub-impact fault makes the rotor running at an unstable speed [2, 25]. In Figs. 15-16, the modes M2 and M3 are the high-order components, which have weak amplitude but show more irregular oscillation characteristics. For instance, the 27.34 Hz and 62.5 Hz cannot be found in mode M1, but they become the dominant motions in the mode M3. It demonstrates that the rub-impact fault should be in the early stage, such that it does not cause violently irregular vibration of the shaft. However, the irregular high-order motion should be paid more attention to avoid the further development of the fault and the occurrence of the major failure. The concentrated TF result provide an effective way to extract the time-varying features of the weak components.

For comparisons, in Fig. 17, we display the logarithm of TF representations generated by SST, RM, second-order SST and forth-order SST, respectively. It can be observed that these TF results are heavily blurry. It is because the conventional SST-based methods cannot provide enough distance to reassign the blurry TF coefficients to the true IF region. Meanwhile, the corresponding Rényi entropies are listed in Table III. It can be concluded that the MSST is able to generate more concentrated TF representation than other TFA methods.

TABLE III  
RÉNYI ENTROPY BY SEVERAL TFA METHODS

TFA	SST	MSST	RM	2nd-SST	4th-SST
Rényi Entropy	13.1045	10.5819	13.132	12.8966	13.5596

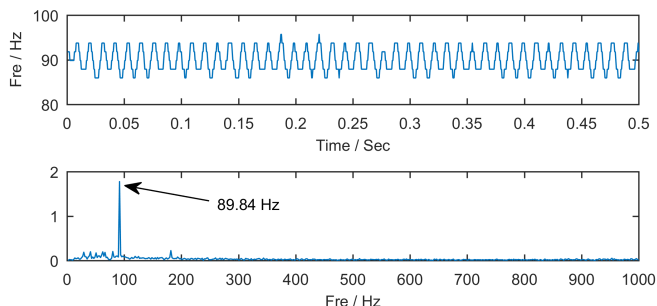


Fig. 14. The detected IF trajectory of mode M1 and its spectrum.

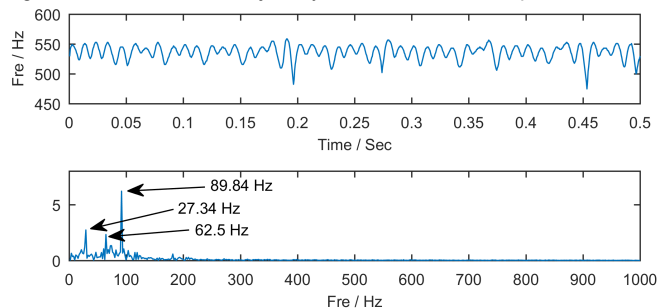


Fig. 15. The detected IF trajectory of mode M2 and its spectrum.

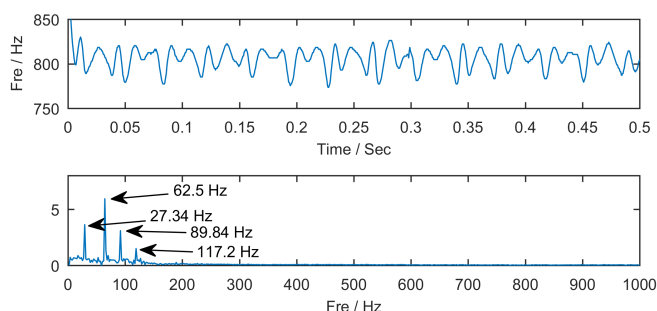


Fig. 16. The detected IF trajectory of mode M3 and its spectrum.

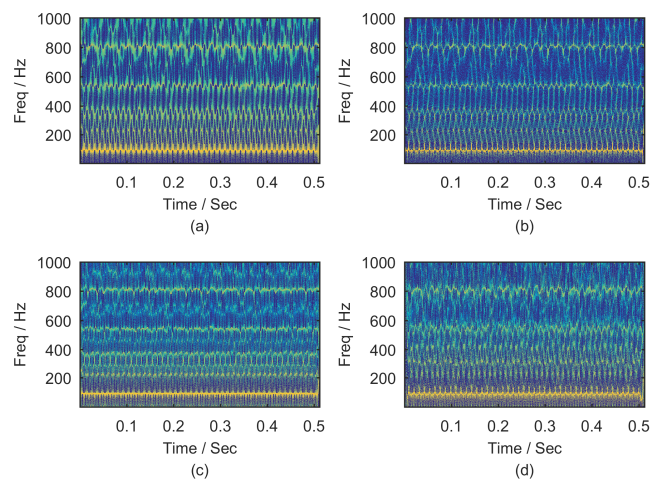


Fig. 17 The logarithm of (a) SST result, (b) RM result, (c) second-order SST result and (d) fourth-order SST result.

### B. Rotating machinery bearing outer race fault vibration signal analysis

In this section, we select the bearing vibration signal with outer race fault to validate the effectiveness of the proposed method. The Case Western Reserve University provides the

data set [26-27]. The structural sketch is shown in Fig. 18, which mainly contains a motor, a torque transducer and a dynamometer. The test bearing is used to support the motor shaft. A heavy fault is introduced to the bearing outer race via electro-discharge machining. Vibration signal is recorded by accelerometers, which is placed at the drive end of the motor housing.

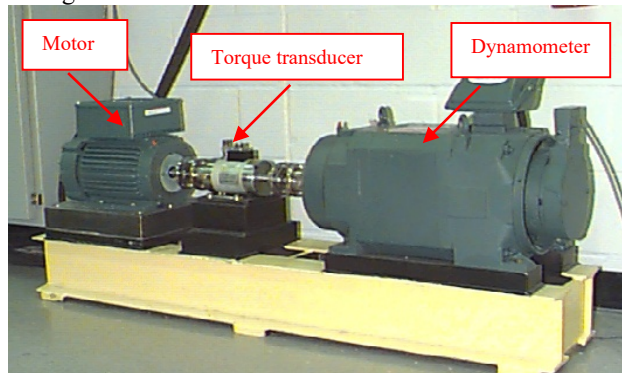


Fig. 18. The structural sketch of the machine set.

The waveform and the frequency spectrum of the vibration signal are plotted in Fig. 19. It can be seen that, the outer race fault results in significantly amplitude-modulated (AM) transient features of the time-series signal. Meanwhile, the spectrum indicates that the main frequency components are around the band 2500 Hz – 4000 Hz.

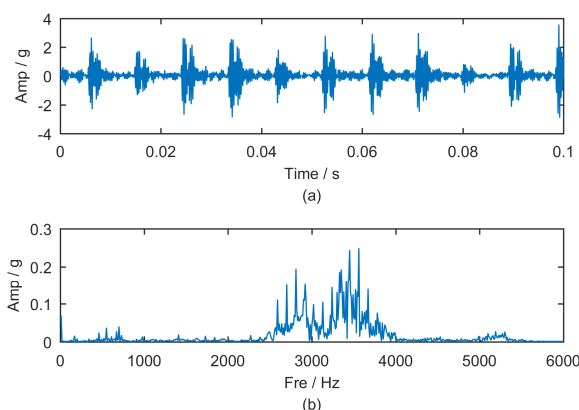


Fig. 19. (a) Waveform and (b) frequency spectrum of the vibration signal.

To reveal more detailed information on the fault, the main focus is on the TF features around 2500 Hz – 4000 Hz. The TF representations generated by STFT, SST, second-order SST, forth-order SST and MSST are displayed in Fig. 20, and the local features are shown in the right side. In Fig. 20(a), the STFT roughly characterize the duration time and the frequency band of each transient component. However, restricted by Heisenberg uncertainty principle, the TF energy of the STFT result smears heavily. In Fig. 20(b), faced with strongly AM signals, the SST fails to provide concentrated result. In Fig. 20(c-d), the high-order SST techniques generate much more concentrated results comparable to the SST. In Fig. 20(e), the MSST provides an obviously concentrated TF result. To evaluate the performance of these methods quantitatively, the Rényi entropies are calculated and listed in Table IV. It is shown that, the SST cannot effectively concentrate the TF

energy comparable to STFT. The high-order SST is more suitable for addressing strongly AM signal than the SST. The MSST result has the lowest Rényi entropy among all TFA methods.

TABLE IV  
RÉNYI ENTROPY BY SEVERAL TFA METHODS

TFA	STFT	SST	2nd-SST	4th-SST	MSST
Rényi Entropy	16.8365	15.0888	13.2646	13.8667	11.2013

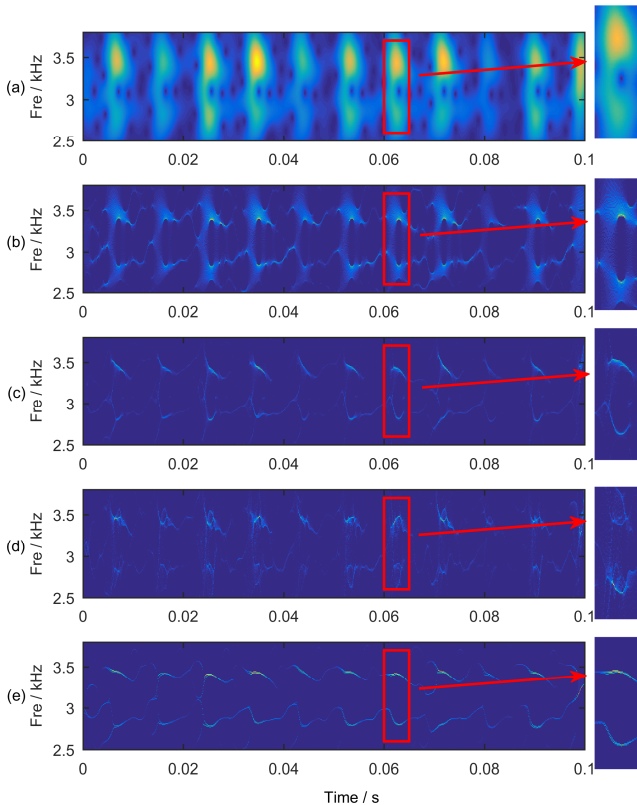


Fig. 20 (a) STFT result, (b) SST result, (c) second-order SST result, (d) fourth-order SST result and (e) MSST result.

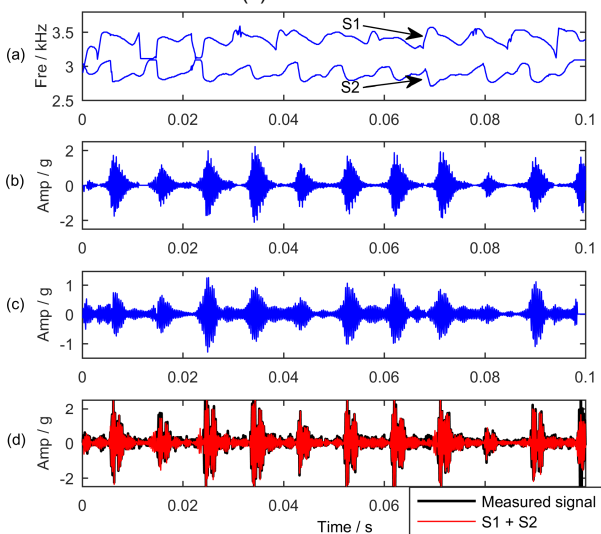


Fig. 21 (a) Detected IFs, (b) mode S1, (c) mode S2 and (d) the superposition of two modes.

In Fig. 20(e), the MSST result obviously shows two oscillated TF trajectories, which denotes that there should be two mono-component modes in the frequency band 2500 Hz – 4000 Hz. According to the MSST result, we can detect two IFs, which is shown in Fig. 21(a). We let S1 and S2 denote these two modes. And then, we can reconstruct the time-series waveform of two modes, which are plotted in Fig. 21(b-c). To validate the reconstructed performance, we also plot the superposition of two modes together with the original signal in Fig. 21(d), which shows that they are highly consistent.

To further reveal the detailed features of two modes, we plot the waveform of two modes together with their IF trajectories in Fig. 22. It is known that, when the motor shaft passes through the fault position of the bearing with heavy defect, it will produce impulse components in a short time, which eventually results in periodic AM transient features in the whole time-series signal [27-29]. From the Fig. 22, it can be also observed that, both of two IFs show periodically oscillated phenomenon, which has the same frequency with the appearance of the AM transient features. It is because that, the defect in the outer race can also decrease the instantaneous speed of the motor shaft, such that it can also cause periodically FM law of the fault frequency in the vibration signal. Therefore, it can be known that, when a heavy failure appears in the bearing, it not only produces periodic AM transient components but periodic FM laws also accompany it. The concentrated TF representation provides a precise way to diagnosis the fault features based on bearing vibration signal.

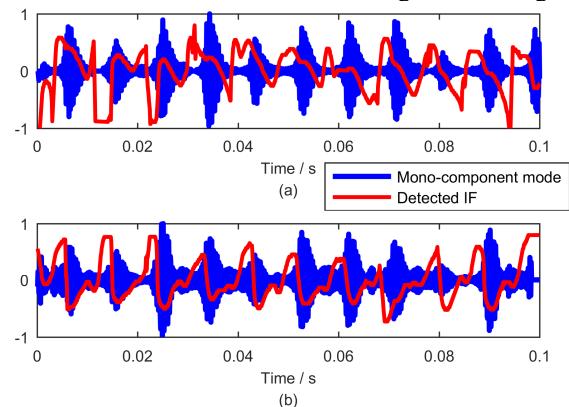


Fig. 22 (a) Waveform of mode S1 and its IF, (b) waveform of mode S2 and its IF.

## V. DISCUSSION

In this section, we mainly focus on the unsolved shortcomings and future development of the MSST technique.

As an iterative algorithm, the MSST needs to be set the termination condition. However, how to stop the iteration is an open issue. If we utilize the Algorithm 1 to implement the MSST, according to the research of Ref. [12], the Rényi entropy can be used for guaranteeing MSST being able to adaptively converge to a satisfactory concentration level. For instance, the iteration procedure can terminate when there are no more evident changes between Rényi entropies of two consecutive TF results in the iterative procedure. According to (32), with the increasing of the iteration number, two adjacent IF estimates will be closer and closer. Therefore, if we utilize

the Algorithm 2 to implement the MSST, we can stop the iteration when the following condition is satisfied,

$$\int_{-\infty}^{+\infty} \int_{-\infty}^{+\infty} |\hat{\omega}^{[N]}(t, \omega) - \hat{\omega}^{[N-1]}(t, \omega)| dt d\omega < \gamma \quad (45)$$

where  $\gamma$  is a small threshold.

According to the expression (32), no matter how many iterations we execute, the IF estimate  $\hat{\omega}^{[N]}(t, \omega)$  of the MSST is always biased for the signal true IF. In addition, if the chirp rate (the second-order derivative of the phase function) of the signal is large, the execution of multiple SST will show less improvement for the IF estimate. In follows, we use the detailed TF features of the numerical signal (42) to illustrate this shortcoming of the MSST. For comparison, the ideal TF representation of the signal (42) is first given in Fig. 23(a), and the local zoom on mode S2 follows in Fig. 23(b). It can be seen that, in each time interval, only one frequency bin appears to describe the mode S2 in the TF plane. The Figs. 23(c-d) provide the MSST result with one hundred iterations. It can be obviously observed that, at time  $t=2.71$  s, there are two TF points. Even if we execute more iterations, these two points cannot be squeezed into one TF point. Furthermore, the amplitude of the TF representation at time  $t=2.71$  s is obviously lower than signal true amplitude. This phenomena is caused by that, the  $\hat{\omega}^{[N]}(t, \omega)$  is always a biased estimate for true IF. Herein, no matter how many iterations are executed, the points that cannot be reassigned into true IF trajectory are named non-reassigned point. How to decrease the number of non-reassigned points is a challenging task. When the non-reassigned points are completely eliminated, the TF result will be definitely equivalent to the ITFA representation.

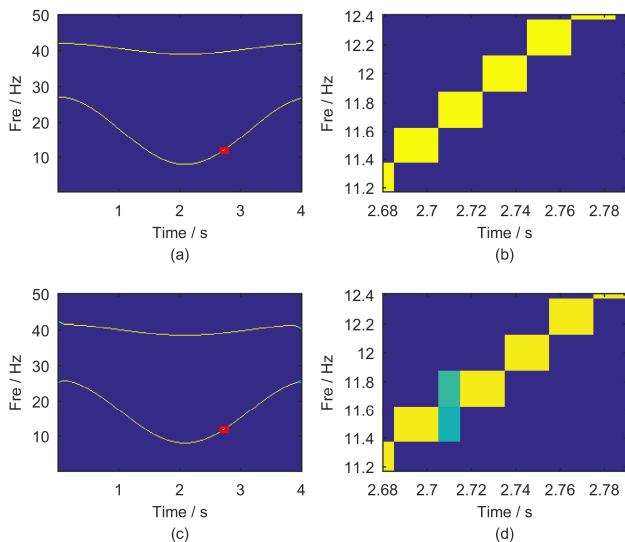


Fig. 23 (a) Ideal TF representation, (b) local zoom on mode S2, (c) MSST result and (d) local zoom on mode S2

The high-order SST is a wonderful technique, which can obtain concentrated TF representation in addressing strongly time-varying signals. For instance, the second-order SST is established on that the signal has linear FM IF. The forth-order SST is established on that the signal has the forth-order polynomial IF. Therefore, the higher-order SST technique should have better performance in addressing the signal with more nonstationary IF. The 2D IF estimate of the MSST is only established on the framework of the SST and is always biased

even for linear FM IF. However, the MSST technique in this paper is not only to provide an algorithm, but also to provide a novel iterative framework for these reassigned methods. A natural development is motivated that, we can construct the IF estimate based on high-order SST, synchrosqueezing WT or synchrosqueezing S transform. Even more, we can propose the iterative procedure for RM technique. In theory, these newly developed methods based on the iterative procedure should have better performance than the original methods. However, the relative theorem should be further explored in the future. Therefore, the proposed MSST technique has large development space and nice application prospects. The MATLAB code that can reproduce all figures in this paper will be available soon on the MATLAB Central website: <https://ww2.mathworks.cn/matlabcentral/fileexchange/68571>.

## VI. CONCLUSION

In this paper, we propose an iterative reassignment procedure to improve the energy concentration of the TF representation by applying multiple SST operation, which is termed MSST. Such a method allows for better addressing a wide variety of multi-component signals containing strongly time-varying laws. The advantages of the proposed technique are also demonstrated through numerical and experimental validations comparable to some advanced methods. The comparisons illustrate that, the proposed method has the better performance in concentrating TF energy and addressing noisy signals than other methods. The experimental analysis demonstrates that, as a benefit of the concentrated TF features, we can recognize the complex physical phenomenon much more precisely.

## REFERENCES

- [1] J. Pons-Llinares et al., "Advanced induction motor rotor fault diagnosis via continuous and discrete time-frequency tools," *IEEE Trans. Ind. Electron.*, vol. 62, no. 3, pp. 1791-1802, Mar. 2015.
- [2] G. Yu et al., "Synchroextracting Transform," *IEEE Trans. Ind. Electron.*, vol. 64, no. 10, pp. 8042-8054, Oct. 2017.
- [3] F. Auger et al., "Time-frequency reassignment and synchrosqueezing: An overview," *IEEE Signal Process. Mag.*, vol. 30, no. 6, pp. 32-41, 2013.
- [4] L.J. Stankovic et al., "An analysis of instantaneous frequency representation using time-frequency distributions-generalized Wigner distribution," *IEEE Trans. Signal Process.*, vol. 43, no. 2, pp. 549-552, 1995.
- [5] L.J. Stanković, et al., "Instantaneous frequency in time-frequency analysis: Enhanced concepts and performance of estimation algorithms," *Digit. Signal Process.*, vol. 35, pp. 1-13, 2014.
- [6] F. Auger and P. Flandrin, "Improving the readability of time-frequency and time-scale representations by the reassignment method," *IEEE Trans. Signal Process.*, vol. 43, no. 5, pp. 1068-1089, 1995.
- [7] I. Daubechies et al., "Synchrosqueezed wavelet transforms: An empirical mode decomposition-like tool," *Appl. Comput. Harmon. Anal.*, vol. 30, no. 2, pp. 243-261, 2011.
- [8] G. Thakur et al., "Synchrosqueezing-based recovery of instantaneous frequency from nonuniform samples,"

- SIAM J. Math. Anal., vol. 43, no. 5, pp. 2078–2095, Sep. 2011.
- [9] Z. Huang et al., “Synchrosqueezing S-transform and its application in seismic spectral decomposition,” *IEEE Trans. Geosci. Remote Sens.*, vol. 54, no. 2, pp. 817–825, 2016.
- [10] Z. K. Peng et al., “Polynomial chirplet transform with application to instantaneous frequency estimation,” *IEEE Trans. Instrum. Meas.*, vol. 60, no. 9, pp. 1378–1384, Sep. 2011.
- [11] Y. Yang, et al., “Multicomponent signal analysis based on polynomial chirplet transform,” *IEEE Trans. Ind. Electron.*, vol. 60, no. 9, pp. 3948–3956, Sep. 2013.
- [12] S. Wang et al., “Matching demodulation transform and synchrosqueezing in time-frequency analysis,” *IEEE Trans. Signal Process.*, vol. 62, no. 1, pp. 69–84, Jan. 2014.
- [13] C. Li et al., “Time-frequency signal analysis for gearbox fault diagnosis using a generalized synchrosqueezing transform,” *Mech. Syst. Signal Process.*, vol. 26, pp. 205–217, 2012.
- [14] T. Oberlin et al., “Second-order synchrosqueezing transform or invertible reassignment? Towards ideal time-frequency representations,” *IEEE Trans. Signal Process.*, vol. 63, no. 5, pp. 1335–1344, Mar. 2015.
- [15] R. Behera et al., “Theoretical analysis of second-order synchrosqueezing transform,” *Appl. Comput. Harmon. Anal.*, in press, 2016.
- [16] D. H. Pham et al., “High-order synchrosqueezing transform for multicomponent signals analysis—With an application to gravitational-wave signal,” *IEEE Trans. Signal Process.*, vol. 65, no. 12, pp. 3168–3178, Jun. 2017.
- [17] S. Wang et al., “Matching Synchrosqueezing Wavelet Transform and Application to Aeroengine Vibration Monitoring,” *IEEE Trans. Instrum. Meas.*, vol. 66, no. 2, pp. 360–372, Jan. 2017.
- [18] S. Wang et al., “Matching synchrosqueezing transform: A useful tool for characterizing signals with fast varying instantaneous frequency and application to machine fault diagnosis,” *Mech. Syst. Signal Process.*, vol. 100, pp.242–288, 2018.
- [19] Hu Y et al., “Joint High-Order Synchrosqueezing Transform and Multi-Taper Empirical Wavelet Transform for Fault Diagnosis of Wind Turbine Planetary Gearbox under Nonstationary Conditions,” *Sensors*, vol. 18, pp.242–288, 2018.
- [20] Y. Yang et al., “General parameterized time–frequency transform,” *IEEE Trans. Signal Process.*, vol. 62, no. 11, pp. 2751–2764, Jun. 2014.
- [21] Feng Z et al., “Adaptive iterative generalized demodulation for nonstationary complex signal analysis: Principle and application in rotating machinery fault diagnosis,” *Mech. Syst. Signal Process.*, vol. 110, pp.1–27, 2018.
- [22] R. Carmona et al., “Multiridge detection and time-frequency reconstruction,” *IEEE Trans. Signal Process.*, vol. 47, no. 2, pp. 480–492, 1999.
- [23] S. Meignen et al., “On demodulation, ridge detection, and synchrosqueezing for multicomponent signals,” *IEEE Trans. Signal Process.*, vol. 65, no. 8, pp. 2093–2103, Apr. 2017.
- [24] S. Chen et al., “Separation of overlapped non-stationary signals by ridge path regrouping and intrinsic chirp component decomposition,” *IEEE Sensors J.*, vol. 17, no. 18, pp. 5994–6005, Sep. 2017.
- [25] S. Wang et al., “Matching demodulation transform with application to feature extraction of rotor rub-impact fault,” *IEEE Trans. Instrum. Meas.*, vol. 63, no. 5, pp. 1372–1383, May 2014.
- [26] S. Wang, et al., “Transient signal analysis based on Levenberg–Marquardt method for fault feature extraction of rotating machines,” *Mech. Syst. Signal Process.*, vol. 54, pp.16–40, 2015.
- [27] W. Smith et al, “Rolling element bearing diagnostics using the Case Western Reserve University data: A benchmark study,” *Mech. Syst. Signal Process.*, vol. 64, pp.100–131, 2015.
- [28] R. Randall et al, “Rolling element bearing diagnostics—A tutorial” *Mech. Syst. Signal Process.*, vol. 25, pp.485–520, 2011.
- [29] S. Wang et al, “Nonconvex Sparse Regularization and Convex Optimization for Bearing Fault Diagnosis,” *IEEE Trans. Ind. Electron.*, vol. 65, no. 9, pp. 7332–7342, 2018.



**Gang Yu** was born in Zhangqiu, China, in 1987. He received the B.Eng. degree in mechanical engineering from Qingdao University, Qingdao, China, in 2010 and the Ph.D. degree in Mechanical Engineering from Shandong University, Jinan, P. R. China, in 2016.

He is currently a Lecturer of Mechanical Engineering with University of Jinan. His current research interests include time-frequency analysis, machinery condition monitoring and fault diagnosis.



**Ping Zhao** received the B.S. degree from the University of Jinan, China, in 2002, the M.S. degree from the Qufu Normal University, China, in 2005, and the Ph.D. from the Academy of Mathematics and Systems Science, Chinese Academy of Sciences. He is currently a teacher of the University of Jinan. His research interests are in the stability theory and control of stochastic and nonlinear systems.



**Zhonghua Wang** received the M.S. degree in Mechanical Engineering from Shandong University and Ph.D. degree in Mechanical Engineering from Southeast University. He is currently a professor of Electrical Engineering with University of Jinan. His current research interests include Nonlinear Control Theory, Modern Control Theory and Computer Simulation Techniques.